



Synthesis and visible-light photocatalytic activity of nanoperovskites and exploration of silver decoration to enhance photocatalytic efficiency

Parvaneh Nakhostin Panahi*, Sara Babaei, Mohammad Hossein Rasoulifard

Department of Chemistry, Faculty of Science, University of Zanjan, Zanjan, Iran, Tel. +982433052477;
emails: panahi@znu.ac.ir (P. Nakhostin Panahi), sarababaei.1991@gmail.com (S. Babaei),
m_h_rasoulifard@znu.ac.ir (M.H. Rasoulifard)

Received 3 June 2019; Accepted 18 March 2020

ABSTRACT

The LaBO_3 (B = Fe, Mn, Co, Ti) and ACoO_3 (A = La, Ca, Sr, Ba) with perovskite structure were prepared by a facile sol–gel method with the aim to study the effect of A and B site ions upon photocatalytic activity. The photocatalytic activity of the perovskites was evaluated by photo-induced discoloration of the malachite green solution under the irradiation of visible light. Our results showed that type A and B cations at perovskite are detrimental to the photocatalytic performance and LaCoO_3 showed the highest photocatalytic activity (44% removal of malachite green at visible light). Then, the effect of substitution of La by Sr and Ba in LaCoO_3 on the structural and photocatalytic properties was investigated. It was found when Ba and Sr are doped on LaCoO_3 , the absorption behavior is markedly enhanced. In the following, Ag was doped in LaCoO_3 by a facile impregnated method in combination with a calcination process, and Ag (2%)/ LaCoO_3 was found to give remarkable photocatalytic activity in the removal of malachite green (80%) compared to pure LaCoO_3 (44%). The effect of Ag-doping in LaCoO_3 on the photocatalytic activity for removal of malachite green has not been reported. The physicochemical properties of the photocatalysts were analyzed by X-ray diffraction, scanning electron microscopy, and UV-visible (diffusive reflectance spectra mode) spectroscopy.

Keywords: Nanoperovskite; Photocatalyst; Dye contaminants; Silver decoration

1. Introduction

With the rapid development of global industrialization, environmental pollutions such as acid rain, depletion of the ozone layer, and smog generation have become the increasing challenges due to the human concern. Nowadays, various techniques have been applied to remove pollutants from wastewater, such as adsorption, ion exchange, biodegradation, and photocatalytic oxidation degradation [1–4]. Among these methods, photocatalytic oxidation with semiconducting materials is a promising method for purification and remediation of polluted water and air, because it can completely degrade most kinds of organic pollutants,

such as dyes and pesticides into harmless substances (such as CO_2 , H_2O , etc.) under moderate conditions and without generating any secondary toxic compounds [5,6]. TiO_2 is the most widely used semiconducting photocatalyst resulting from its prominent characteristics, such as excellent photocatalytic activity, thermal stability, low cost, and non-toxicity [7]. However, its practical application has not yet reached a satisfying extent due to its wide bandgap (3.2 eV) that only can absorb the ultraviolet (UV) light occupying a small fraction (<6%) of the solar energy [8]. Since the visible light accounts for the largest portion (ca. 46%) in the solar spectrum, the development of visible-light-driven photocatalysts is an important challenge in order to

* Corresponding author.

utilize solar radiation as an energy source for photocatalysis. In recent years, a new type of semiconductor material with a perovskite structure has been exploited as an effective photocatalyst in the visible region [9]. Perovskite oxides with the general formula ABO_3 have been known as an important kind of multifunctional material exhibiting a variety of interesting properties, such as electronic transport, dielectric properties, low cost, environmental friendliness, and catalytic activity [10,11]. Depending on A and B cations type, the ABO_3 perovskites present many applications, such as catalysts [12], electrode material in fuel cells [13], electrocatalysts for O_2 evolution [14], perovskite based solar cells [15] and photo/electrocatalysts for dyes degradation [16]. Further, substitution or doping at both A and B sites can change the composition and symmetry of the oxide and create cations or oxygen vacancies, which enhance the catalytic properties of perovskite oxides [17–19]. Among perovskite oxides, $LaCoO_3$ has attracted considerable attention due to its prominent catalytic activity and thermal stability [20]. In recent years, much research has been done on catalytic properties of $LaCoO_3$ [12], but its photocatalytic activity is rarely reported. In $ACoO_3$ ($A = La, Ca, Sr, Ba$), ions of A-site certainly influence photocatalytic activity due to the distinction of ion radius, so it is necessary to investigate the influence of A-site in $ACoO_3$ on the photocatalytic activity.

Among modification methods of the photocatalyst, doping with noble metals has attracted significant attention to improve photocatalytic performance [21]. Noble metals such as Pt, Pd, Au, and Ag had electron storage property, consequently can act as charge transfer sites and prevent/delay photoelectron-hole pairs from fast recombination and hence, improve the photocatalytic performance [22,23]. Compared with the expensive Pt, Pd, Rh, and Au noble metals, Ag is more attractive due to its non-toxicity and the work function of Ag is much lower which favors the formation of good band alignment [24,25]. Pan et al. [26] reported that an Ag microgrid connected TiO_2 nanocrystalline film enhanced the photocatalytic degradation of methylene blue. To the best of our knowledge, the effect of Ag-doping in $LaCoO_3$ on the photocatalytic activity for removal of malachite green has not been reported in the research literature.

Based on above considerations, in this paper as new photocatalytic materials, $LaBO_3$ ($B = Fe, Mn, Co, Ti$) and $ACoO_3$ ($A = La, Ca, Sr, Ba$) were synthesized by the sol-gel method and their photocatalytic performances compared for the decomposition of malachite green under visible-light irradiation. Then the effect of the partial substitution of La by Sr and Ba on the photocatalytic activity and adsorption properties of $LaCoO_3$ investigated. In addition, the improvement effect of Ag-doping in $LaCoO_3$ on the photocatalytic activity and also appropriate content of Ag doping explored.

2. Materials and methods

2.1. Synthesis of nanoperovskites

2.1.1. Synthesis of $LaBO_3$ ($B = Fe, Mn, Co, Ti$) and $ACoO_3$ ($A = La, Ca, Sr, Ba$) perovskites

The nanoperovskites with different substituents on the B-site ($B = Fe, Mn, Co, Ti$) and on the A-site (La, Ca, Sr, Ba) were prepared using pechini type sol-gel method.

The detail process is as follows: The required precursors in the suitable molar equivalents were dissolved in deionized water under stirring to form clear homogeneous solution. The citric acid as chelating-fuel agent (at a molar ratio of 2:1 with respect to the cations) and ethylene glycol as esterifiable reagent (in 3:1 molar ratio of ethylene glycol to citric acid) were added into solution. After that, the resulting mixture was heated and continuously stirred at $70^\circ C$ to promote esterification between ethylene glycol and citric acid, to obtain sticky gel. After the gel was placed in an oven at $200^\circ C$ until it turned into a porous dried gel. Then the dried gel was grinded and calcined at $700^\circ C$ for 6 h to obtain single phase perovskite [12,27].

2.1.2. Synthesis of $La_{0.8}A'_{0.2}CoO_3$ ($A' = Ba$ and Sr) perovskites

The $La_{0.8}A'_{0.2}CoO_3$ ($A' = Ba$ and Sr) nanoperovskites were also prepared by pechini type sol-gel method. The synthesis condition was similar to that of $LaCoO_3$, just stoichiometric amount of barium and strontium nitrates also was added in deionized water and other steps continued the same.

2.1.3. Synthesis of silver-modified $LaCoO_3$ perovskites

$Ag/LaCoO_3$ nanoperovskites with various mol % of silver (1%, 2%, 4%, 7%, and 10%) were synthesized using incipient wetness method. Briefly, silver nitrate ($AgNO_3$) solution with required concentration was prepared for Ag doping in $LaCoO_3$. Then 1 g of $LaCoO_3$ powder was dispersed in $AgNO_3$ solution with stirring and the resulting suspension evaporated. Afterwards, the resulting solid was dried at $100^\circ C$ overnight and taken to calcination at $450^\circ C$ for 2 h and Finally, the $Ag/LaCoO_3$ obtained [28,29].

2.2. Characterization

The crystalline phase structure and morphology of the obtained samples were characterized by scanning electron microscopy (SEM, LEO 1430VP, Germany) and X-ray diffraction (XRD, D500 Ziemence, USA) with $Cu K\alpha$ radiation ($V = 35$ kV). To study the light absorption of the catalysts, the diffusive reflectance spectra (DRS) of the prepared catalysts in the wavelength range of 290–800 nm obtained by using a UV-vis spectrophotometer (Scinco, S4100-00-0701001U, Korea).

2.3. Photocatalysis and adsorption tests

The photocatalytic activity of the prepared samples was investigated by the degradation of malachite green under visible light irradiation. During the photocatalytic tests, 4 mg of the catalyst was added to a glass beaker containing 100 mL malachite green solution (10 ppm) and commercially available LED lamp (32 W) used as the visible light source (the spectrum of the LED lamp is at supplement data). The suspension was exposed to light irradiation for 5.5 h under magnetic stirring. Every 1 h, 5 mL of suspension was taken from the reaction beaker and after centrifugation and filtering of the suspension; the concentration of the malachite green was determined by measuring the absorbance at 615 nm on a spectrophotometer. One test was performed

under the similar conditions without photocatalyst for the measurement of the photolysis and adsorption test was also performed without visible irradiation. The discoloration percentage (%) was calculated as follows:

$$(\%) = \frac{(C_0 - C_t)}{C_0} \times 100 \quad (1)$$

where C_0 and C_t represent the initial and final concentration, respectively.

3. Results and discussion

3.1. Characterization of photocatalysts

3.1.1. XRD analysis

Fig. 1 shows XRD patterns taken from LaCoO_3 and $\text{La}_{0.8}\text{Sr}_{0.2}\text{CoO}_3$ powders. The substituted sample ($\text{La}_{0.8}\text{Sr}_{0.2}\text{CoO}_3$) has peaks similar to the unsubstituted sample (LaCoO_3), indicating that the crystal structure has not changed after Sr doping. All of the diffraction lines were matched well with the JCPDS Card: 00-025-1060 confirming the formation of the perovskite structure [30]. The sharp diffraction peaks of $\text{La}_{0.8}\text{Sr}_{0.2}\text{CoO}_3$ indicate that Sr^{2+} being substituted by La^{3+} induced an increase in the crystallinity. The diffraction peaks of both samples are comparatively broad which is likely related to the small particle size of as-prepared nanoperoovskites [31]. The average crystallite size of both perovskites was calculated using Scherrer's equation to be in the range 14–19 nm.

The XRD patterns of LaCoO_3 before and after modification by Ag are illustrated in Fig. 2. The Ag modified LaCoO_3 ($\text{Ag}(2\%)/\text{LaCoO}_3$) show the diffraction peaks with position similar to LaCoO_3 and full width at half-maximum, suggesting that the crystallite size and structure of LaCoO_3 were not affected by the Ag modification processes. No obvious diffraction peak belong to Ag phase observed, that this is due to a small amount of Ag in the catalyst structure [32]. Further, a detailed analysis of the diffraction pattern of $\text{Ag}(2\%)/\text{LaCoO}_3$ shows a splitting in peak of $2\theta = 33^\circ$. This splitting approves the incorporation of Ag⁺ ions into the perovskite structure.

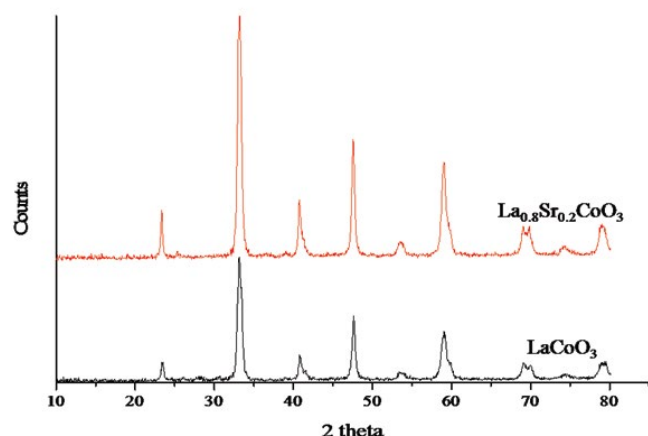


Fig. 1. XRD patterns of LaCoO_3 and $\text{La}_{0.8}\text{Sr}_{0.2}\text{CoO}_3$.

3.1.2. SEM analysis

The SEM was used to examine the size and morphology of LaCoO_3 before and after modification by Ag and after photocatalysis and the SEM images are shown in Fig. 3. According to Fig. 3a, the particles of LaCoO_3 have spherical structures with smooth surface and compact stacking and also have a uniform size distribution. After modification by Ag to form the $\text{Ag}(2\%)/\text{LaCoO}_3$ (Fig. 3b), the surface morphology and size of the particles have no obvious change and the LaCoO_3 and $\text{Ag}(2\%)/\text{LaCoO}_3$ exhibit similar morphologies. However, according to the SEM images, less agglomeration degree is observed for $\text{Ag}(2\%)/\text{LaCoO}_3$ compared with that of the pure LaCoO_3 . The SEM image of $\text{Ag}(2\%)/\text{LaCoO}_3$ after photocatalysis (Fig. 3c) show any transform in surface morphology. Consequently, photocatalysis reactions don't change morphology, agglomeration degree and size of particles and photocatalyst is stable. The micrographs also indicate that LaCoO_3 and $\text{Ag}(2\%)/\text{LaCoO}_3$ are nanosized with size ranges from 40 to 60 nm.

Additional information regarding the presence of metals in $\text{Ag}(2\%)/\text{LaCoO}_3$ obtained from SEM-EDS (energy-dispersive X-ray spectroscopy) profile, Fig. 4. The appearance of Ag peak in the EDS profile of $\text{Ag}(2\%)/\text{LaCoO}_3$ indicate its presence in the perovskite. Finally, the spectrum confirmed the corresponding chemical elements for catalyst compound and no other elements were detected.

3.1.3. Transmission electron microscopy analysis

The transmission electron microscopy (TEM) images of LaCoO_3 and $\text{Ag}(2\%)/\text{LaCoO}_3$ photocatalysts are presented in Fig. 5. The nanosized and well-dispersed particles can be clearly observed for both samples.

3.1.4. Optical absorption properties

The optical response and band-gap energy of the semiconductors play crucial role in the effectiveness of the photocatalytic activity. The photocatalysis process is the direct absorption of photon by band of the materials and generates electron-hole pairs in the semiconductor materials. Indeed, the excitation of an electron from the valence band

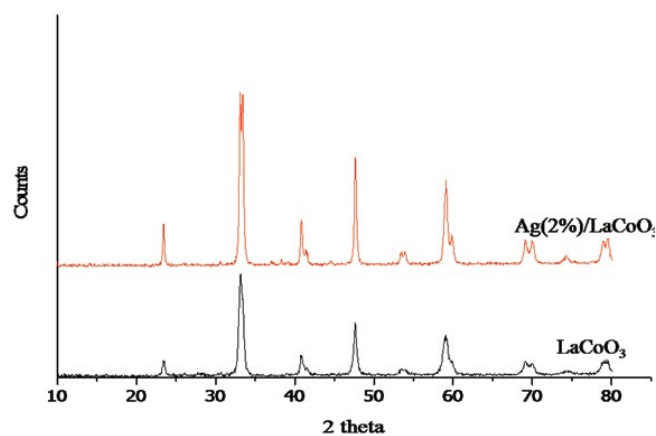


Fig. 2. XRD patterns of LaCoO_3 and $\text{Ag}(2\%)/\text{LaCoO}_3$.

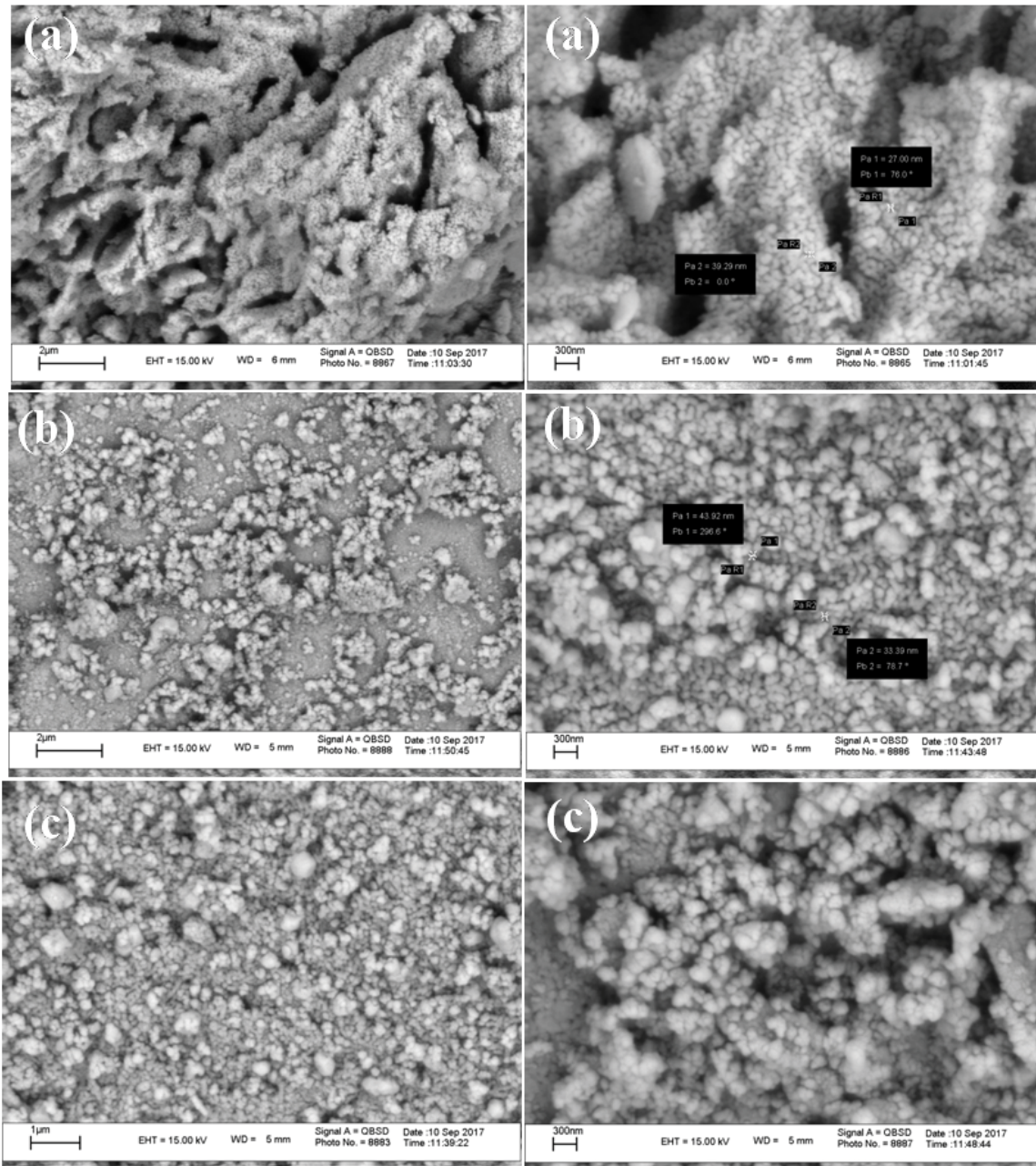


Fig. 3. SEM images of (a) LaCoO₃, (b) fresh Ag (2%)/LaCoO₃, and (c) Ag (2%)/LaCoO₃ after photocatalysis.

to the conduction band is possible by light absorption with energy equal to or greater than the band-gap of the semiconductor [33]. The optical properties of the LaCoO₃ and Ag (2%)/LaCoO₃ were investigated by UV-vis diffuse reflectance spectroscopy, and the results are shown in Fig. 6. It is observed that the absorption cut off wavelength of both samples is around 750 nm suggesting that the present materials can efficiently absorb visible light and consequently they show potential application as visible-light-driven photocatalysts. After doping of Ag (Ag (2%)/LaCoO₃), the absorption band exhibited slight enhancement in the whole visible-light region.

The optical absorption coefficient near the band edge follows the equation $\alpha h\nu = A(h\nu - E_{bg})^{n/2}$, where α , h , ν , E_{bg} , and A are absorption coefficient, Planck constant, light frequency, band-gap energy, and a constant, respectively. The corresponding band-gap energy of samples can be obtained from the plot of $(\alpha h\nu)^2$ vs, $h\nu$ by extrapolating the straight portion of $(\alpha h\nu)^2$ to zero [34], as shown in Fig. 6b. After calculation, the values were estimated to be 2.75 and 2.67 eV for LaCoO₃ and Ag (2%)/LaCoO₃, respectively. Such narrow band-gap is advantageous for the efficient utilization of visible light for photocatalysis. In addition, the lowering of the band gap of Ag (2%)/LaCoO₃ relative

to parent LaCoO_3 is due to the doping energy level of $\text{Ag}(\text{I})$ ion in the LaCoO_3 lattice [35]. This fact suggests an increase in the number of electron–hole pairs, which can participate in the photocatalytic reaction [36]. Consequently, it can be expected that the $\text{Ag} (2\%)/\text{LaCoO}_3$ show enhanced photocatalytic activity relative to LaCoO_3 .

3.2. Adsorptive and photocatalytic activities of the prepared samples

To differentiate between the absorption, photocatalysis, and photolysis of malachite green, experiments were carried out in the presence or absence of visible light irradiation and catalyst under identical conditions.

3.2.1. Test of LaBO_3 ($B = \text{Co}, \text{Mn}, \text{Ti}, \text{Fe}$) and ACoO_3 ($A = \text{La}, \text{Sr}, \text{Ba}$) samples

Fig. 7 shows the photolysis, absorption and photo-degradation of malachite green in the presence of LaBO_3 ($B = \text{Co}, \text{Mn}, \text{Ti}, \text{Fe}$) catalysts. From the pattern, the degradation

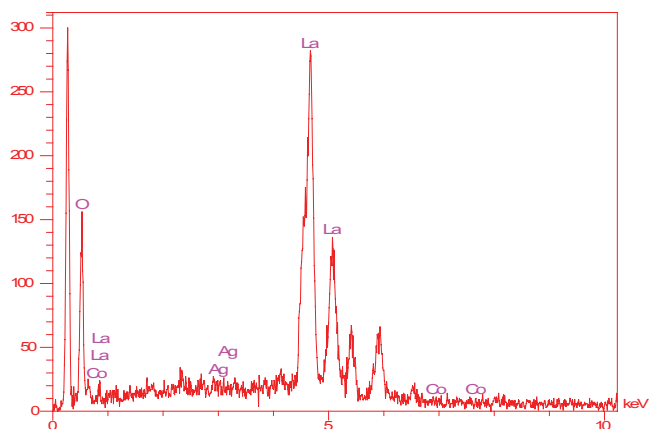


Fig. 4. EDS profile of $\text{Ag} (2\%)/\text{LaCoO}_3$.

of malachite green was found to be only 1.5% after lighting for 5.5 h without catalyst. Therefore, it reveals a mild photo-decomposition effect in the removal of dye. The removal of malachite green via adsorption by the LaBO_3 ($B = \text{Co}, \text{Mn}, \text{Ti}, \text{Fe}$) catalysts (dark test) is presented in Fig. 7a and was found to be slightly. The results of photocatalytic activity of LaBO_3 catalysts are shown at Fig. 7b. According to this figure, the degradation of malachite green significantly increased with the LaBO_3 under visible light irradiation and LaCoO_3 showed the highest photocatalytic decolorization (44%).

As observed in the absence of only catalysts or only light, the removal of malachite green is slightly, indicating that the direct photolysis and the adsorption of malachite green is partial and removal of malachite green only proceeds via the photo-excited semiconductor catalyst. Consequently, the presence of both illumination and photocatalyst are necessary for the efficient removal of malachite green.

Fig. 8 exhibits the absorption and photo-degradation of malachite green in the presence of ACoO_3 ($A = \text{La}, \text{Sr}, \text{Ba}$) catalysts under dark and light irradiation, respectively. According to Fig. 8a, the quantity of adsorbed malachite green by BaCoO_3 , CaCoO_3 , and SrCoO_3 was found to be 75.2%, 72.5%, and 86.5%, respectively. This shows that they have excellent adsorptive capacity for malachite green. With substitution Sr and Ba instead of La, crystal lattice defects create and act as absorption centers and thus adsorptive capacity for malachite green increases. A comparison of discoloration due to adsorption (Fig. 8a) and discoloration due to photocatalysis (Fig. 8b) reveals that LaCoO_3 has the highest photocatalytic activity. Therefore, LaCoO_3 was selected to investigate the effect of alkaline earth metals-doping on the photocatalytic activity of LaCoO_3 for the decomposition of dye.

3.2.2. Test of $\text{La}_{0.8}\text{A}'_{0.2}\text{CoO}_3$ ($\text{A}' = \text{Sr}, \text{Ba}$) samples

Fig. 9 shows the effect of the alkaline earth metals doping on the activity of LaCoO_3 . As shown in the Fig. 8a, the $\text{La}_{0.8}\text{Sr}_{0.2}\text{CoO}_3$ and $\text{La}_{0.8}\text{Ba}_{0.2}\text{CoO}_3$ have high adsorption

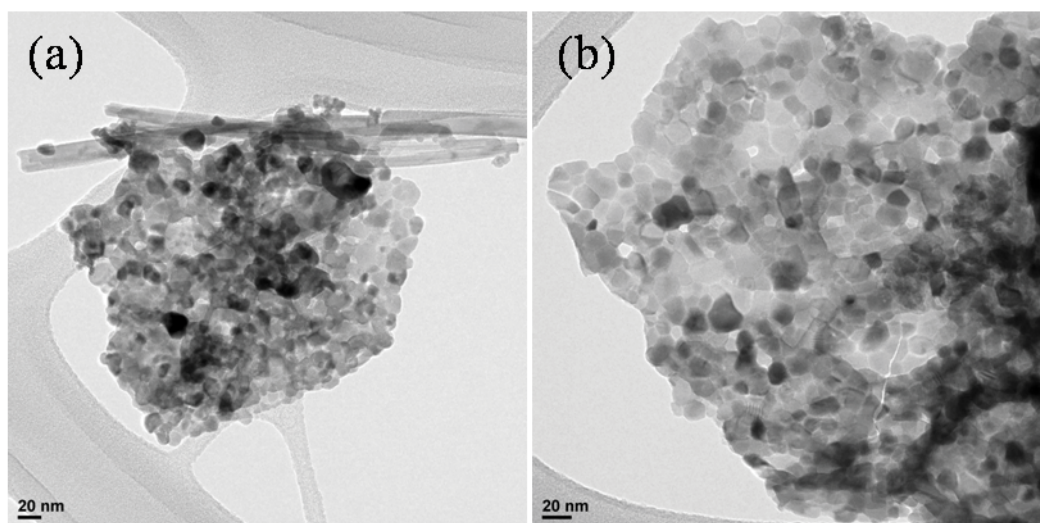


Fig. 5. TEM images of (a) LaCoO_3 and (b) $\text{Ag}(2\%)/\text{LaCoO}_3$.

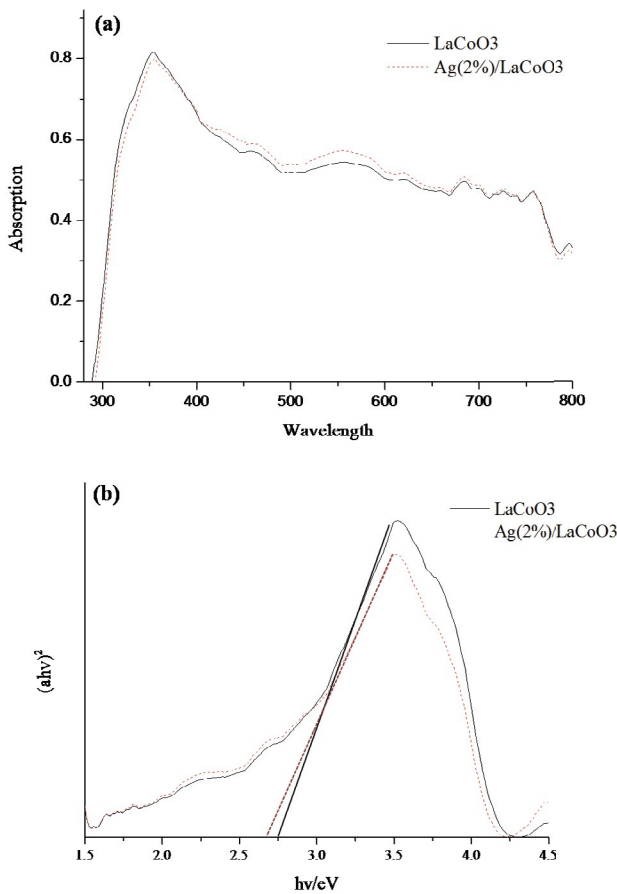


Fig. 6. UV-vis diffuse reflectance spectra of LaCoO₃ and Ag (2%)/LaCoO₃.

property, and 45% and 47.8% of the dye was adsorbed, respectively. Indeed, the results of Figs. 9a and b indicate that the alkaline earth metals doping in the LaCoO₃ have a great effect upon absorption behavior, but photocatalytic activity of is not increased.

The possible reason may be due to the further holes that are created in the crystal structure when trivalent La atoms are replaced by divalent Ba and Sr. The holes act as absorption centers for dye pollution and lead to an increase in absorption behavior of catalyst [16].

3.2.3. Test of Ag/LaCoO₃ samples

To improve the photocatalytic activity of LaCoO₃, Ag was doped with various amounts (from 1% to 7%) in LaCoO₃ (Ag is able to sever as an electron collector) and results are shown at Fig. 10. Modification of LaCoO₃ with Ag caused a remarkable increase in the photocatalytic activity for decomposition of dye. While the degradation of dye increased with the addition of Ag 1% and 2%, the degradation declined with higher amounts of Ag. However, increasing the doping amount very much, the catalytic activity is always decreased due to accumulation of the active center. Therefore, there is an optimal value of the doping of active component [37]. In this study, the maximum activity obtained for LaCoO₃ with doping 2% of the Ag (Ag (2%)/LaCoO₃). The possible

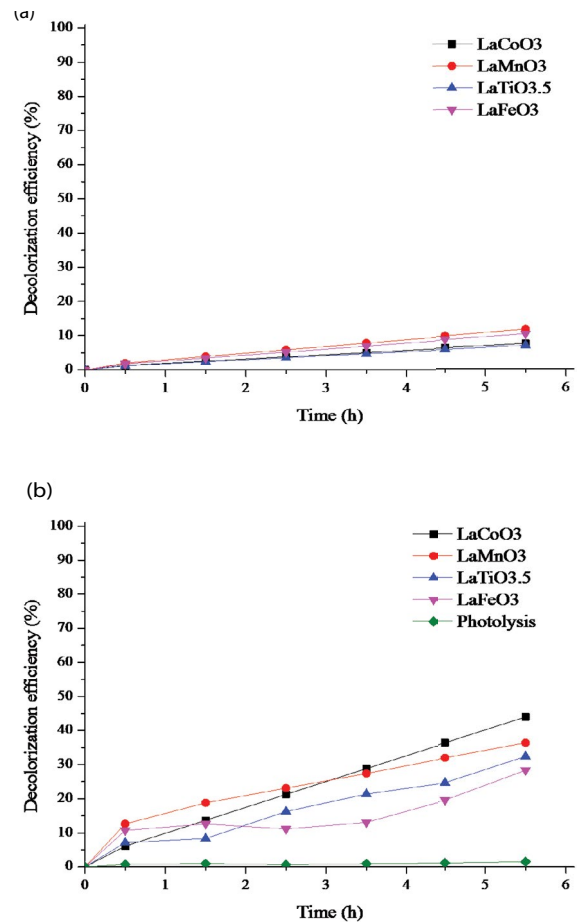


Fig. 7. Decolorization of malachite green by LaBO₃ (B = Co, Mn, Ti, Fe) under (a) dark condition and (b) visible light irradiation (C_0 (dye) = 10 mg L⁻¹, catalyst dose = 40 mg L⁻¹).

reaction mechanism has been proposed to explain the excellent photocatalytic activity of Ag (2%)/LaCoO₃. Considering that a number of Ag⁺ ions are impregnated into the lattice of LaCoO₃ during the calcination process, Ag-4d orbital can have a great effect on the valence band of LaCoO₃. Actually, the narrowing of band-gap of Ag (2%)/LaCoO₃ (according to Fig. 6) can be attributed to the formation of an isolated energy level of Ag-4d in the band gap [35]. In addition to, the metallic Ag deposited on the surface of LaCoO₃ efficiently captures the photogenerated electrons at conduction band and supplies them for react with O₂ adsorbed on the surface of the catalyst. The corresponding holes remained in valence band also react with OH⁻ to create OH[•]. These OH[•] and O₂^{•-} radicals can oxidize the dye contamination into CO₂ and H₂O [28,37]. Therefore, the high photocatalytic activity of Ag (2%)/LaCoO₃ (80%) is owing to the formation of an isolated energy level of Ag-4d in the band gap of LaCoO₃ leading to decrease in band gap energy and also the metallic Ag nanoparticles deposited on the surface of LaCoO₃ promote the effective separation of the electron-hole pairs, resulting in the high visible-light photocatalytic activity [38].

Alharbi and Abdelrahman [39] studied the degradation of malachite green dye under the influence of UV using hematite nanoparticles and 46.29% of dye degraded.

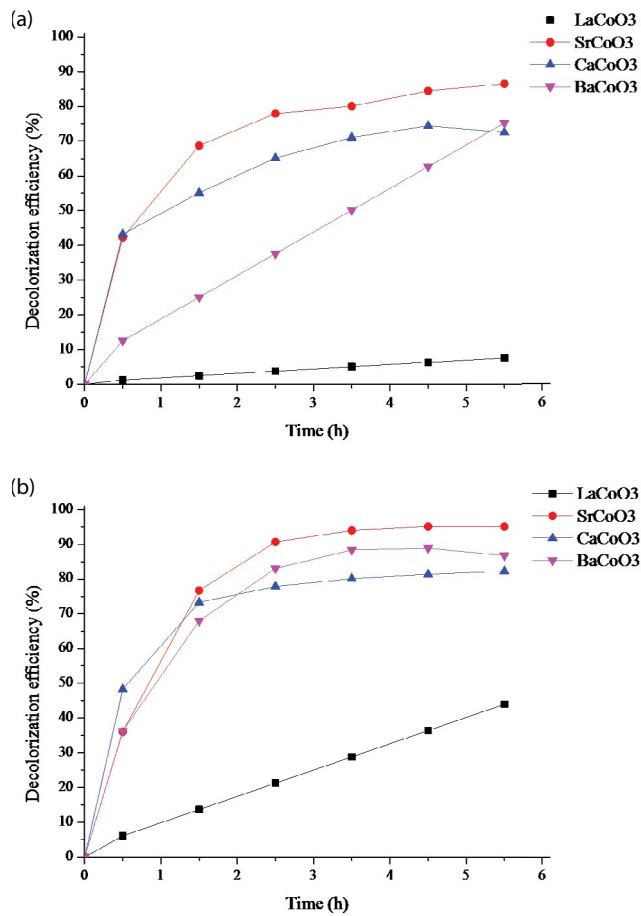


Fig. 8. Decolorization of malachite green by $ACoO_3$ ($A = La, Sr, Ca, Ba$) under (a) dark condition and (b) visible light irradiation ($C_0(\text{dye}) = 10 \text{ mg L}^{-1}$, catalyst dose = 40 mg L^{-1}).

Khparde and Acharya [40] synthesized isovalent (Mn, Cd, Cu, Co)-doped-ZnS nanoparticles by co-precipitation route and their photocatalytic activity for decoloration of malachite green dyes was tested in visible radiation under natural conditions. The results indicated that 65% of dye is degraded. Therefore, comparison between the photocatalytic efficiency of Ag (2%)/LaCo₃ and other photocatalysts proves that Ag (2%)/LaCo₃ photocatalyst is more efficient for the degradation of malachite green dye.

Based on the literature reports [41,42], a relevant mechanism for the photocatalytic activity of lanthanide perovskite could be expressed according to detailed reaction steps as follows:

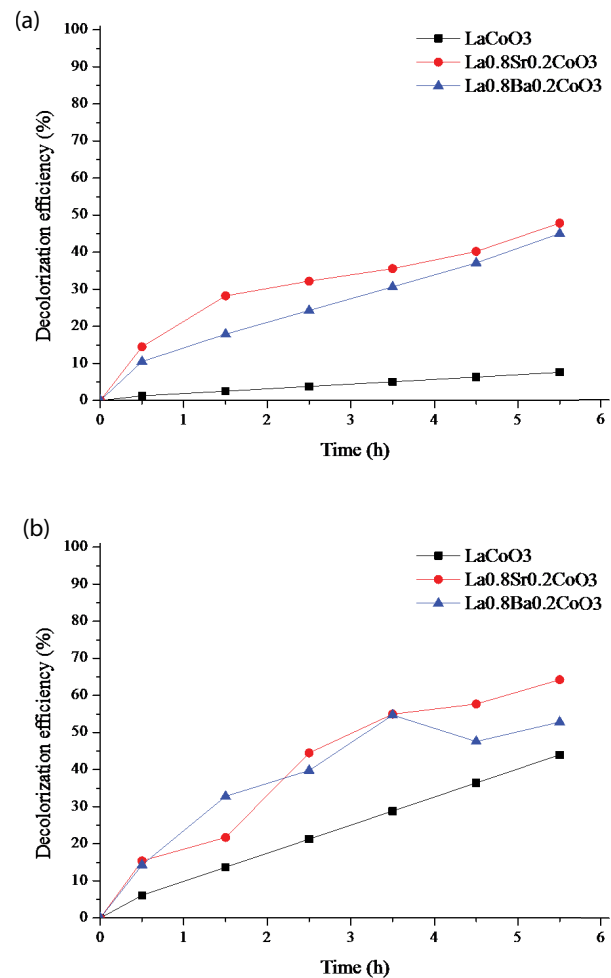
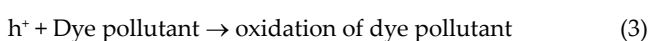


Fig. 9. Decolorization of malachite green by LaCo₃, La_{0.8}Sr_{0.2}Co₃ and La_{0.8}Ba_{0.2}Co₃ under (a) dark condition and (b) visible light irradiation ($C_0(\text{dye}) = 10 \text{ mg L}^{-1}$, catalyst dose = 40 mg L^{-1}).



4. Conclusion

In conclusion, we have successfully synthesized the LaBO₃ ($B = Fe, Mn, Co, Zn$) and $ACoO_3$ ($A = La, Ca, Sr, Ba$) by sol-gel method and the activity of all samples was evaluated for the removal of malachite green. The results showed that the LaBO₃ ($B = Fe, Mn, Co, Zn$) catalysts have photocatalytic activity for degradation of malachite green under visible light irradiation and the $ACoO_3$ ($A = La, Ca, Sr, Ba$) catalysts have excellent adsorptive capacity for malachite green. A comparison of the discoloration during the photocatalytic test with the discoloration due to adsorption

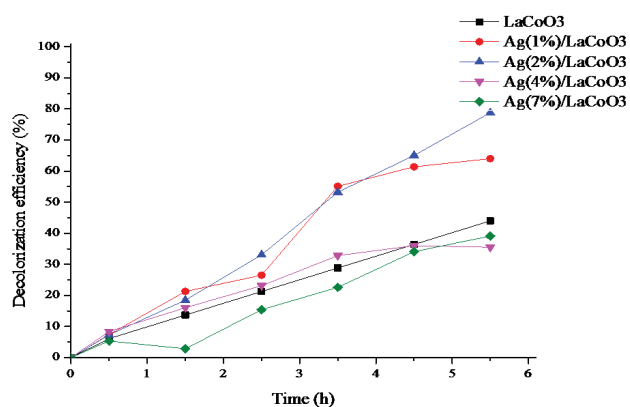


Fig. 10. Effect of Ag content on the photocatalytic decolorization of malachite green by Ag/LaCoO₃ under visible light irradiation (C_0 (dye) = 10 mg L⁻¹, catalyst dose = 40 mg L⁻¹).

revealed that LaCoO₃ has the highest photocatalytic activity. The partial substitution of La by Sr and Ba in LaCoO₃ increased absorption behavior. The influence of Ag decoration in LaCoO₃ on photocatalytic activity was investigated and the highest decolorization efficiency (80%) was obtained by Ag (2%)/LaCoO₃ under the irradiation of visible light. The synthesized samples were systematically characterized by XRD, SEM, and UV-vis (DRS mode) spectroscopy. The SEM images showed that LaCoO₃ and Ag (2%)/LaCoO₃ possess sphere like morphology and average particles size was about 50 nm. This study provided an extremely promising photocatalyst for cleaning wastewater by using visible light.

Acknowledgments

The authors would like to acknowledge the financial support from University of Zanjan and Iranian Nanotechnology Initiative.

References

- [1] G. Sharma, B. Thakur, M. Naushad, A. Kumar, F.J. Stadler, S.M. Alfadul, G.T. Mola, Applications of nanocomposite hydrogels for biomedical engineering and environmental protection, *Environ Chem Lett.*, 16 (2018) 113–146.
- [2] G. Sharma, M. Naushad, D. Pathania, A. Kumar, Multifunctional nanocomposite pectin thorium(IV) tungstomolybdate for heavy metal separation and photoremediation of malachite green, *Desal. Water Treat.*, 57 (2016) 19443–19455.
- [3] G. Sharma, B. Thakur, M. Naushad, H. Aláa, A. Kumar, M. Sillanpää, G.T. Mola, Fabrication and characterization of sodium dodecyl sulphate@iron silicophosphate nanocomposite: ion exchange properties and selectivity for binary metal ions, *Mater. Chem. Phys.*, 193 (2017) 129–139.
- [4] G. Sharma, S. Bhogal, M. Naushad, A. Kumar, F.J. Stadler, Microwave assisted fabrication of La/Cu/Zr/carbon dots trimetallic nanocomposites with their adsorption vs. photocatalytic efficiency for remediation of persistent organic pollutants, *J. Photochem. Photobiol., A*, 347 (2017) 235–243.
- [5] S. Fukahori, H. Ichiura, T. Kitaoka, H. Tanaka, Capturing of bisphenol A photodecomposition intermediates by composite TiO₂-zeolite sheets, *Appl. Catal., B*, 46 (2003) 453–462.
- [6] D. Bahnemann, S. Kholuiskaya, R. Dillert, A. Kulak, A. Kokorin, Photodestruction of dichloroacetic acid catalyzed by nano-sized TiO₂ particles, *Appl. Catal., B*, 36 (2002) 161–169.
- [7] N. Yao, K.L. Yeung, Investigation of the performance of TiO₂ photocatalytic coatings, *Chem. Eng. J.*, 167 (2011) 13–21.
- [8] M. Li, Z. Hong, Y. Fang, F. Huang, Synergistic effect of two surface complexes in enhancing visible-light photocatalytic activity of titanium dioxide, *Mater. Res. Bull.*, 43 (2008) 2179–2186.
- [9] S.W. Bae, S.M. Ji, S.J. Hong, J.W. Jang, J.S. Lee, Photocatalytic overall water splitting with dual-bed system under visible light irradiation, *Int. J. Hydrogen Energy*, 34 (2009) 3243–3249.
- [10] S. Fu, H. Niu, Z. Tao, J. Song, C. Mao, S. Zhang, C. Chen, D. Wang, Low temperature synthesis and photocatalytic property of perovskite-type LaCoO₃ hollow spheres, *J. Alloys Compd.*, 576 (2013) 5–12.
- [11] S.N. Tijare, M.V. Joshi, P.S. Padole, P.A. Mangrulkar, S.S. Rayalu, N.K. Labhsetwar, Photocatalytic hydrogen generation through water splitting on nano-crystalline LaFeO₃ perovskite, *Int. J. Hydrogen Energy*, 37 (2012) 10451–10456.
- [12] S.A. Hosseini, D. Salari, A. Niaei, S.A. Oskoui, Physical-chemical property and activity evaluation of LaB_{0.5}Co_{0.5}O₃ (B = Cr, Mn, Cu) and LaMn_{1-x}Co_xO₃ (x = 0.1, 0.25, 0.5) nano perovskites in VOC combustion, *J. Ind. Eng. Chem.*, 19 (2013) 1903–1909.
- [13] W. Zhou, R. Ran, Z. Shao, Progress in understanding and development of Ba_{0.5}Sr_{0.5}Co_{0.8}Fe_{0.2}O_{3-δ}-based cathodes for intermediate-temperature solid-oxide fuel cells: a review, *J. Power Sources*, 192 (2009) 231–246.
- [14] A. Costa, M.M. Jorge, M. Carvalho, A. Gomes, M. da Silva Pereira, LaNi_{1-x}Cu_xO₃ (x = 0.05, 0.10, 0.30) coated electrodes for oxygen evolution in alkaline medium, *J. Solid State Electrochem.*, 17 (2013) 2311–2318.
- [15] P. Tonui, S.O. Oseni, G. Sharma, Q. Yan, G.T. Mola, Perovskites photovoltaic solar cells: an overview of current status, *Renewable Sustainable Energy Rev.*, 91 (2018) 1025–1044.
- [16] M. Bradha, T. Vijayaraghavan, S. Suriyaraj, R. Selvakumar, A.M. Ashok, Synthesis of photocatalytic La_(1-x)A_xTiO_{3-δ} (A = Ba, Sr, Ca) nano perovskites and their application for photocatalytic oxidation of congo red dye in aqueous solution, *J. Rare Earths*, 33 (2015) 160–167.
- [17] R. Hammami, H. Batis, C. Minot, Combined experimental and theoretical investigation of the CO₂ adsorption on LaMnO_{3-y} perovskite oxide, *Surf. Sci.*, 603 (2009) 3057–3067.
- [18] L. Han, C. Chen, H. Dong, J. Wang, G. Gao, Effect of Al doping on the magnetic and electrical properties of layered perovskite La_{1-x}Sr_xMn_{1-x}Al_xO₇, *Physica B*, 403 (2008) 2614–2617.
- [19] Z.-X. Wei, C.-M. Xiao, W.-W. Zeng, J.-P. Liu, Magnetic properties and photocatalytic activity of La_{0.8}Ba_{0.2}Fe_{0.9}Mn_{0.1}O_{3-δ} and LaFe_{0.9}Mn_{0.1}O_{3-δ}, *J. Mol. Catal. A: Chem.*, 370 (2013) 35–43.
- [20] W.Y. Jung, S.-S. Hong, Synthesis of LaCoO₃ nanoparticles by microwave process and their photocatalytic activity under visible light irradiation, *J. Ind. Eng. Chem.*, 19 (2013) 157–160.
- [21] T. Puangpetch, T. Sreehawong, S. Chavadej, Hydrogen production over metal-loaded mesoporous-assembled SrTiO₃ nanocrystal photocatalysts: effects of metal type and loading, *Int. J. Hydrogen Energy*, 35 (2010) 6531–6540.
- [22] X. Yang, L. Xu, X. Yu, Y. Guo, One-step preparation of silver and indium oxide co-doped TiO₂ photocatalyst for the degradation of rhodamine B, *Catal. Commun.*, 9 (2008) 1224–1229.
- [23] P. Wang, B. Huang, X. Qin, X. Zhang, Y. Dai, M.-H. Whangbo, Ag/AgBr/WO₃·H₂O: visible-light photocatalyst for bacteria destruction, *Inorg. Chem.*, 48 (2009) 10697–10702.
- [24] D. Lin, H. Wu, R. Zhang, W. Pan, Enhanced photocatalysis of electrospun Ag-ZnO heterostructured nanofibers, *Chem. Mater.*, 21 (2009) 3479–3484.
- [25] Y. You, L. Wan, S. Zhang, D. Xu, Effect of different doping methods on microstructure and photo-catalytic activity of Ag₂O-TiO₂ nanofibers, *Mater. Res. Bull.*, 45 (2010) 1850–1854.
- [26] F. Pan, J. Zhang, W. Zhang, T. Wang, C. Cai, Enhanced photocatalytic activity of Ag microgrid connected TiO₂ nanocrystalline films, *Appl. Phys. Lett.*, 90 (2007) 122114.
- [27] R. Hu, C. Li, X. Wang, Y. Sun, H. Jia, H. Su, Y. Zhang, Photocatalytic activities of LaFeO₃ and La₂FeTiO₆ in p-chlorophenol degradation under visible light, *Catal. Commun.*, 29 (2012) 35–39.

- [28] Z. Wang, K. Teramura, S. Hosokawa, T. Tanaka, Photocatalytic conversion of CO₂ in water over Ag-modified La₂Ti₂O₇, *Appl. Catal., B*, 163 (2015) 241–247.
- [29] P.N. Panahi, A. Niaei, D. Salari, S. Mousavi, Selective catalytic reduction of NO over M–Ag/ZSM-5 bimetallic nanocatalysts (M = Mn, Fe and Ni). Physicochemical properties and catalytic performance, *Kinet. Catal.*, 56 (2015) 617–624.
- [30] L. Wang, Q. Pang, Q. Song, X. Pan, L. Jia, Novel microbial synthesis of Cu doped LaCoO₃ photocatalyst and its high efficient hydrogen production from formaldehyde solution under visible light irradiation, *Fuel*, 140 (2015) 267–274.
- [31] S. Feraru, A. Borhan, P. Samoila, C. Mita, S. Cucu-Man, A. Iordan, M. Palamaru, Development of visible-light-driven Ca₂Fe_{1-x}Sm_xBiO₆ double perovskites for decomposition of Rhodamine 6G dye, *J. Photochem. Photobiol., A*, 307 (2015) 1–8.
- [32] A. Abbasi, M. Hamadianian, M. Salavati-Niasari, S. Mortazavi-Derazkola, Facile size-controlled preparation of highly photocatalytically active ZnCr₂O₄ and ZnCr₂O₄/Ag nanostructures for removal of organic contaminants, *J. Colloid Interface Sci.*, 500 (2017) 276–284.
- [33] Y. Wei, X. Zhang, J. Xu, J. Wang, Y. Huang, L. Fan, J. Wu, Enhancement of photocatalytic activity from HCa₂Ta₁Nb_{3-x}O₁₀ (x = 0, 1), co-intercalated with sulfides particles, *Appl. Catal., B*, 147 (2014) 920–928.
- [34] W. Wang, N. Li, Y. Chi, Y. Li, W. Yan, X. Li, C. Shao, Electrospinning of magnetical bismuth ferrite nanofibers with photocatalytic activity, *Ceram. Int.*, 39 (2013) 3511–3518.
- [35] R. Liu, P. Wang, X. Wang, H. Yu, J. Yu, UV-and visible-light photocatalytic activity of simultaneously deposited and doped Ag/Ag(I)-TiO₂ photocatalyst, *J. Phys. Chem. C*, 116 (2012) 17721–17728.
- [36] B. Barrocas, S. Sério, A. Rovisco, Y. Nunes, M.M. Jorge, Removal of rhodamine 6G dye contaminant by visible light driven immobilized Ca_{1-x}Ln_xMnO₃ (Ln = Sm, Ho; 0.1 ≤ x ≤ 0.4) photocatalysts, *Appl. Surf. Sci.*, 360 (2016) 798–806.
- [37] N. Zhao, S. Li, X. Zhang, X. Huang, J. Wang, R. Gao, J. Zhao, J. Wang, Photocatalytic performances of Ag/ALa₄Ti₄O₁₅ (A = Ca, Sr and Ba) on H₂O₂ oxidative desulfurization, *Colloids Surf., A*, 481 (2015) 125–132.
- [38] S. Jayapandi, D. Lakshmi, S. Premkumar, P. Packiyaraj, K. Anitha, Augmented photocatalytic and electrochemical activities of Ag tailored LaCoO₃ perovskite semiconductor, *Mater. Lett.*, 218 (2018) 205–208.
- [39] A. Alharbi, E.A. Abdelrahman, Efficient photocatalytic degradation of malachite green dye using facily synthesized hematite nanoparticles from Egyptian insecticide cans, *Spectrochim. Acta, Part A*, 226 (2020) 117612.
- [40] R. Khaparde, S. Acharya, Effect of isovalent dopants on photodegradation ability of ZnS nanoparticles, *Spectrochim. Acta, A*, 163 (2016) 49–57.
- [41] M. Rasoulifard, M.S. Dorraji, S. Taherkhani, Photocatalytic activity of zinc stannate: preparation and modeling, *J. Taiwan Inst. Chem. Eng.*, 58 (2016) 324–332.
- [42] H. Jie, M. Jie, M. Jiahua, H. Huang, Preparation of LaMnO₃/graphene thin films and their photocatalytic activity, *J. Rare Earths*, 32 (2014) 1126–1134.

Supplementary information

